their sites of action. Often, these anchored enzymes only become activated when their stimulating second messengers and signals become available. Recent data suggest that serine phosphorylation, like tyrosine phosphorylation, may directly regulate modular protein-protein interactions. Now that the intricacy of these interactions is understood, the challenge ahead is to understand both the physiological functions and regulation of such signaling networks.

REFERENCES AND NOTES

1. D. Anderson *et al.*, *Science* **250**, 979 (1990).
2. T. Pawson, *Nature* **373**, 573 (1995); G. B. Cohen, R. Ren, D. Baltimore, *Cell* **80**, 237 (1995).
3. M. Hubbard and P. Cohen, *Trends Biochem. Sci.* **18**, 172 (1993); D. Mochly-Rosen, *Science* **268**, 247 (1995); M. C. Faux and J. D. Scott, *Trends Biochem. Sci.* **21**, 312 (1996).
4. M. C. Faux and J. D. Scott, *Cell* **85**, 8 (1996).
5. Z. Songyang *et al.*, *ibid.* **72**, 767 (1993); G. Waksman *et al.*, *ibid.*, p. 779; S. M. Pascal *et al.*, *ibid.* **77**, 461 (1994).
6. F. Maina *et al.*, *ibid.* **87**, 531 (1996).
7. P. Blaikie *et al.*, *J. Biol. Chem.* **269**, 32031 (1994); W. M. Kavanaugh and L. T. Williams, *Science* **266**, 1862 (1994); T. A. Gustafson *et al.*, *Mol. Cell. Biol.* **15**, 2500 (1995).
8. Single-letter abbreviations for the amino acid residues are as follows: A, Ala; C, Cys; D, Asp; E, Glu; F, Phe; G, Gly; H, His; I, Ile; K, Lys; L, Leu; M, Met; N, Asn; P, Pro; Q, Gln; R, Arg; S, Ser; T, Thr; V, Val; W, Trp; and Y, Tyr. X indicates any amino acid.
9. P. van der Geer *et al.*, *Curr. Biol.* **5**, 404 (1995); W. M. Kavanaugh, C. W. Turck, L. T. Williams, *Science* **268**, 1177 (1995).
10. T. Trub *et al.*, *J. Biol. Chem.* **270**, 18205 (1995); P. van der Geer *et al.*, *Proc. Natl. Acad. Sci. U.S.A.* **93**, 963 (1996).
11. M. M. Zhou *et al.*, *Nature* **378**, 584 (1995).
12. J. P. Borg, J. Ooi, E. Levy, B. Margolis, *Mol. Cell. Biol.* **16**, 6229 (1996); S. C. Li *et al.*, *Proc. Natl. Acad. Sci. U.S.A.* **94**, 7204 (1997).
13. D. A. Doyle *et al.*, *Cell* **85**, 1067 (1996).
14. E. Kim *et al.*, *Nature* **378**, 85 (1995); Z. Songyang *et al.*, *Science* **275**, 73 (1997).
15. J. S. Simske *et al.*, *Cell* **85**, 195 (1996).
16. J. Chevesich, A. J. Kreuz, C. Montell, *Neuron* **18**, 95 (1997); H.-C. Kornau, L. T. Schenker, M. B. Kennedy, P. H. Seeburg, *Science* **269**, 1737 (1995); H. Dong *et al.*, *Nature* **386**, 279 (1997); P. R. Brakeman *et al.*, *ibid.*, p. 284.
17. N. A. Cohen *et al.*, *Neuron* **17**, 759 (1996).
18. Y. Hsueh, E. Kim, M. Sheng, *ibid.* **18**, 803 (1997).
19. M. Irie *et al.*, *Science* **277**, 1511 (1997).
20. J. E. Brenman *et al.*, *Cell* **84**, 757 (1996).
21. B. Shieh and M. Zhu, *Neuron* **16**, 991 (1996).
22. S. Tsunoda *et al.*, *Nature* **388**, 243 (1997).
23. S. Feng, J. K. Chen, H. Yu, J. A. Simon, S. L. Schreiber, *Science* **266**, 1241 (1994).
24. D. Chen *et al.*, *J. Biol. Chem.* **271**, 6328 (1996).
25. M. Sudol, *Prog. Biophys. Mol. Biol.* **65**, 113 (1996); M. J. Macias *et al.*, *Nature* **382**, 646 (1996).
26. M. T. Bedford *et al.*, *EMBO J.* **16**, 2376 (1997).
27. P. M. Snyder *et al.*, *Cell* **83**, 969 (1995).
28. R. Ranganathan *et al.*, *ibid.* **89**, 875 (1997).
29. M. B. Yaffe *et al.*, *Science* **278**, 1957 (1997).
30. K. Niebuhr *et al.*, *EMBO J.* **16**, 5433 (1997).
31. J. E. Harlan *et al.*, *Nature* **371**, 168 (1994); M. A. Lemmon *et al.*, *Proc. Natl. Acad. Sci. U.S.A.* **92**, 10472 (1995).
32. A. Toker and L. Cantley, *Nature* **387**, 673 (1997).
33. J. K. Klarlund *et al.*, *Science* **275**, 1927 (1997); P. Chardin *et al.*, *Nature* **384**, 481 (1996).
34. K. Salim *et al.*, *EMBO J.* **15**, 6241 (1996); M. Fukuda *et al.*, *J. Biol. Chem.* **271**, 30303 (1996).
35. M. Vihinen *et al.*, *FEBS Lett.* **413**, 205 (1997); M. Hyvonen and M. Saraste, *EMBO J.* **16**, 3396 (1997).
36. X. J. Sun *et al.*, *Mol. Cell. Biol.* **13**, 7418 (1993).
37. L. Yenush *et al.*, *J. Biol. Chem.* **271**, 24300 (1996).
38. K. M. Weidner *et al.*, *Nature* **384**, 173 (1996); Y. Yamanashi and D. Baltimore, *Cell* **88**, 205 (1997); N. Carpino *et al.*, *ibid.*, p. 197; S. J. Holland *et al.*, *EMBO J.* **16**, 3877 (1997).
39. H. Kouhara *et al.*, *Cell* **89**, 693 (1997).
40. P. van der Geer *et al.*, *Curr. Biol.* **6**, 1435 (1996).
41. T. Raabe *et al.*, *Cell* **85**, 911 (1996).
42. M. L. Dell'Acqua and J. D. Scott, *J. Biol. Chem.* **272**, 12881 (1997).
43. T. Gao *et al.*, *Neuron* **19**, 185 (1997).
44. C. Rosenmund *et al.*, *Nature* **368**, 853 (1994); B. D. Johnson, T. Scheuer, W. A. Catterall, *Proc. Natl. Acad. Sci. U.S.A.* **91**, 11492 (1994).
45. L. B. Lester, L. K. Langeberg, J. D. Scott, *Proc. Natl. Acad. Sci. U.S.A.*, in press.
46. L. J. Huang *et al.*, *J. Biol. Chem.* **272**, 8057 (1997).
47. K. A. Burton *et al.*, *Proc. Natl. Acad. Sci. U.S.A.* **94**, 11067 (1997).
48. V. M. Coghlan *et al.*, *Science* **267**, 108 (1995); T. M. Klauck *et al.*, *ibid.* **271**, 1589 (1996); J. B. Nauert *et al.*, *Curr. Biol.* **7**, 52 (1997).
49. D. Mochly-Rosen, H. Khaner, J. Lopez, *Proc. Natl. Acad. Sci. U.S.A.* **88**, 3997 (1991); C. Chapline *et al.*, *J. Biol. Chem.* **268**, 6858 (1993).
50. J. Staudinger *et al.*, *J. Cell Biol.* **128**, 263 (1995).
51. N. K. Tonks and B. G. Neel, *Cell* **87**, 365 (1997); L. J. Mauro and J. E. Dixon, *Trends Biochem. Sci.* **19**, 151 (1994).
52. M. J. Hubbard *et al.*, *Eur. J. Biochem.* **189**, 243 (1990).
53. M. P. Egloff *et al.*, *EMBO J.* **16**, 1876 (1997).
54. D. F. Johnson *et al.*, *Eur. J. Biochem.* **239**, 317 (1996).
55. J. A. Printen, M. J. Brady, A. R. Saltiel, *Science* **275**, 1475 (1997).
56. E. Sontag *et al.*, *Neuron* **17**, 1201 (1996).
57. F. Shibasaki, E. R. Price, D. Milan, F. McKeon, *Nature* **382**, 370 (1996); C. Loh *et al.*, *J. Biol. Chem.* **271**, 10884 (1996).
58. C. J. Marshall, *Cell* **80**, 179 (1995).
59. I. Herskowitz, *ibid.*, p. 187.
60. K.-Y. Choi *et al.*, *Cell* **78**, 499 (1994); J. A. Printen and G. F. Sprague Jr., *Genetics* **138**, 609 (1994); S. Marcus *et al.*, *Proc. Natl. Acad. Sci. U.S.A.* **91**, 7762 (1994).
61. M. S. Whiteway *et al.*, *Science* **269**, 1572 (1995).
62. D. Yablonski, I. Marbach, A. Levitzki, *Proc. Natl. Acad. Sci. U.S.A.* **93**, 13864 (1996).
63. L. Bardwell and J. Thorner, *Trends Biochem. Sci.* **21**, 373 (1996).
64. F. Posas and H. Saito, *Science* **276**, 1702 (1997).
65. M. Dickens *et al.*, *ibid.* **277**, 693 (1997).
66. D. Morrison, *ibid.* **266**, 56 (1994).
67. B. Xiao *et al.*, *Nature* **376**, 188 (1995); D. Liu *et al.*, *ibid.*, p. 191.
68. S. Braselmann and F. McCormick, *EMBO J.* **14**, 4839 (1995).
69. A. J. Muslin *et al.*, *Cell* **84**, 889 (1996); H. M. Xing, K. Kornfeld, A. J. Muslin, *Curr. Biol.* **7**, 294 (1997).
70. C.-Y. Peng *et al.*, *Science* **277**, 1501 (1997).
71. J. Zha *et al.*, *Cell* **87**, 619 (1996).
72. G. Moorhead *et al.*, *Curr. Biol.* **6**, 1104 (1996).

73. T.P. is a Terry Fox Cancer Scientist of the National Cancer Institute of Canada and J.D.S. is supported by NIH grant GM48231. We thank R. Frank for technical assistance. Because of space limitations, we were not able to acknowledge the contributions of all investigators to this growing field.

RESEARCH ARTICLES

Large-Cage Zeolite Structures with Multidimensional 12-Ring Channels

Xianhui Bu, Pingyun Feng, Galen D. Stucky

Zeolite type structures with large cages interconnected by multidimensional 12-ring (rings of 12 tetrahedrally coordinated atoms) channels have been synthesized; more than a dozen large-pore materials were created in three different topologies with aluminum (or gallium), cobalt (or manganese, magnesium, or zinc), and phosphorus at the tetrahedral coordination sites. Tetragonal UCSB-8 has an unusually large cage built from 64 tetrahedral atoms and connected by an orthogonal channel system with 12-ring apertures in two dimensions and 8-ring apertures in the third. Rhombohedral UCSB-10 and hexagonal UCSB-6 are structurally related to faujasite and its hexagonal polymorph, respectively, and have large cages connected by 12-ring channels in all three dimensions.

Extensive research has led to the synthesis of zeolitic materials with previously unseen compositions and framework topologies (*1*), including ultralarge-pore structures VPI-5, $AlPO_4$-8, and UTD-1, which have pores formed of 18-, 14-, and 14-rings, respectively (*2*). A number of structures with 12-ring channels (for example, $AlPO_4$-5, MAPSO-46, and CoAPO-50) have also been reported (*1*). Other open framework structures that have large cages or pore sizes include JDF-20, cloverite (*3*), and unusually low-density vanadium phosphate frameworks (*4*).

Unlike faujasite or its hexagonal polymorph, known materials with a zeolite

X. Bu and P. Feng are in the Department of Chemistry and G. D. Stucky is in the Department of Chemistry and Department of Materials, University of California, Santa Barbara, CA 93106, USA.

structure—such as VPI-5, $AlPO_4$-8, UTD-1, and most 12-ring structures—have channels with the largest pore size in only one dimension (*1*). Some of these structures have no other channels intersecting the main channel, which can be less desirable for commercial applications because of diffusion limitations.

Multidimensional 12-ring channel systems with large cages are highly desirable structural features for industrial applications. Various ion forms (Na, Ca, and Li) of zeolite X have been used as air-separation adsorbents for gas production (*5*). In the petroleum industry, one of the most widely used catalysts for a variety of oil refining processes is zeolite Y. Both zeolites X and Y have the faujasite type structure. Unfortunately, structures with large cages connected by multidimensional 12-ring channel systems are rare (*1*). Until now, only two zeolite structure types (FAU for faujasite and EMT for its hexagonal polymorph) were known to have large cages connected by a three-dimensional (3D) 12-ring channel system. Another zeolite structure with a 3D 12-ring channel system is zeolite beta, but it cannot be prepared as a pure polymorph and has no cages (*6*).

We previously reported an approach that resulted in the synthesis of many new small-pore, transition-metal–based zeolite structure analogs (*7*). It is, however, also desirable to have a methodology for synthesizing multidimensional large-pore structures. A survey of currently known zeolite structure types suggests that large cages and multidimensional channel systems are more commonly found in structures with a relatively high framework charge density. For example, compared to zeolites with a low Si-to-Al ratio, molecular sieves with a high Si-to-Al ratio have a stronger tendency to form structures with nonintersecting channels and no large cages (*8*). Similarly in phosphates, frameworks with a low charge density, such as VPI-5, $AlPO_4$-8, $AlPO_4$-5, and $AlPO_4$-31, have 1D channels, whereas those with a higher framework charge density, such as CoAPO-50, MAPSO-46, and DAF-1, have small or medium-sized pore channels intersecting main channels (*9*).

The focus of this study is the synthesis of zeolite structures with large cages interconnected by multidimensional large-pore channels by means of structure direction through host-guest charge-density matching in the highly charged phosphate system. When the charge density of the organic groups closely approximates that of the inorganic framework that is being formed, direct structural templating takes place in which at least one point group symmetry element of the templating molecule determines the crystallographic point group symmetry of the framework (*10*). The specific template-framework species interaction used in these studies is that between a primary or secondary ammonium cation and an oxygen anion coordinated to tetrahedrally coordinated atoms (T atoms) in solution that translates into the N–H···O interaction in the final host-guest condensed framework structure. The charge on the inorganic framework is adjusted to the organic template charge by restructuring the framework assembly. This alteration can be accomplished by (i) adjusting the curvature and charge of the framework surrounding the template through the creation of expanded or interrupted cages or, (ii) if tetrahedral atoms with different charges (for example, Al^{3+} and Co^{2+}) are made available during the assembly, matching framework charge with template charge by appropriately changing the framework composition. Here we chose the second method, letting the charge requirements of the organic template determine the framework composition and charge. The cobalt aluminophosphate system is attractive because a large concentration of Co^{2+} can be incorporated into the framework Al^{3+} sites to give structures with a relatively high framework charge density (*7*). Thus, the framework charge is readily varied from −1 to 0 for each MPO_4 unit. The synthesis method developed from the cobalt aluminophosphate system has been extended to other systems such as Mg, Mn, or Zn alumino- (or gallo-) phosphate systems with similar framework charge densities. Water solvation and hydrolysis reactions with transition elements are serious competing interactions that can lead to interrupted and nonzeolitic frameworks, so that a partially nonaqueous media is preferred.

The generation of configurations with large cages and pores requires additional domain separation of the charged wall from the cage and core contents. They can be separated by templating with an organic molecule that has spatially competing hydrophilic and hydrophobic regions. We initially used protonated dibutylamine, with its relatively large hydrophobic group, as a structure-directing agent, which successfully led to the synthesis of a cobalt aluminophosphate faujasite analog (*7*). Primary, secondary, and tertiary amines were previously unknown to be able to direct the formation of the faujasite topology. A more effective and controlled method of introducing spatially competing regions is through the use of gemini type molecules (*11*). In this study, we selected the related linear diamines, $NH_2(CH_2)_nNH_2$ ($n \geq 7$), and polyether diamines with backbones that have a smaller affinity than the amine groups for the charged inorganic species that ultimately makes up the framework wall (*12*). These diamines are flexible enough to give by folding relatively high charge densities at the template-framework interface. The polyether diamines are par-

Table 1. Summary of crystallographic data for selected zeolite analogs and structures synthesized in this study. $R(F) = \Sigma||F_o| - |F_c||/\Sigma|F_o|$, with $F_o > 4.0\sigma(F_o)$; $2\Theta_{max}$ refers to the maximum 2Θ value (MoKα radiation) in degrees for reflections used in the structure refinement; M-O is the average bond distance for all unique metal atom sites in each structure. Unit cell β angles for monoclinic crystals: ACP-PHI2, 90.946°; CAP-AEI2, 90.087°. In the formulas: $0.4 < x < 0.5$; $0.3 < y < 0.5$; R1 = $(CH_3)_2CHNH(CH_2)_3NHCH(CH_3)_2$; R2= $[(NH_2(CH_2)_3)]_2NH$; and R3 = 5-amino-1,3,3-trimethylcyclohexanemethylamine. All amines are fully protonated in crystal structures.

Name	Structural formula	Space group	*a* (Å)	*b* (Å)	*c* (Å)	*R*(*F*)	$2\Theta_{max}$ (deg)	M-O (Å)
UCSB-6GaCo	$Co_xGa_{1-x}PO_4$	$P\bar{3}1c$	17.836	17.836	27.182	7.04	45	1.878
UCSB-6GaMg	$Mg_xGa_{1-x}PO_4$	$P\bar{3}1c$	17.859	17.859	27.149	7.16	45	1.864
UCSB-6GaZn	$Zn_xGa_{1-x}PO_4$	$P\bar{3}1c$	17.843	17.843	27.198	8.31	45	1.870
UCSB-6Co	$Co_{0.45}Al_{0.55}PO_4$	$P\bar{3}1c$	17.701	17.701	27.349	8.63	45	1.824
UCSB-6Mn	$Mn_xAl_{1-x}PO_4$	$P\bar{3}1c$	17.817	17.817	27.531	8.77	45	1.856
UCSB-6Mg	$Mg_xAl_{1-x}PO_4$	$P\bar{3}1c$	17.700	17.700	27.352	11.2	45	1.812
UCSB-6Zn	$Zn_xAl_{1-x}PO_4$	$P\bar{3}1c$	17.688	17.688	27.396	10.9	45	1.831
UCSB-8Co	$Co_xAl_{1-x}PO_4$	*P4/nnc*	19.065	19.065	27.594	9.85	44	1.810
UCSB-8Mn	$Mn_xAl_{1-x}PO_4$	*P4/nnc*	19.390	19.390	27.067	11.8	44	1.854
UCSB-8Mg	$Mg_xAl_{1-x}PO_4$	*P4/nnc*	19.090	19.090	27.486	12.3	44	1.805
UCSB-8Zn	$Zn_xAl_{1-x}PO_4$	*P4/nnc*	18.999	18.999	27.958			
UCSB-10GaZn	$ZnGaP_2O_8$	$R\bar{3}$	18.080	18.080	41.951	4.51	50	1.897
UCSB-10Co	$Co_xAl_{1-x}PO_4$	$R\bar{3}$	17.704	17.704	41.690	8.75	50	1.819
UCSB-10Mg	$Mg_xAl_{1-x}PO_4$	$R\bar{3}$	17.661	17.661	41.608	11.3	45	1.800
UCSB-10Zn	$Zn_xAl_{1-x}PO_4$	$R\bar{3}$	17.625	17.625	41.581			
CAP-RHO1	$(R1)Co_2Al_2P_4O_{16}$	*I*23	15.480	15.480	15.480	6.49	56	1.822
MnAP-RHO1	$(R1)Mn_2Al_2P_4O_{16}$	*I*23	15.610	15.610	15.610	9.34	45	1.869
MAP-RHO1	$(R1)Mg_2Al_2P_4O_{16}$	*I*23	15.552	15.552	15.552	7.67	50	1.811
ACP-PHI2	$(R2)Al_yCo_{1-y}PO_4$	*C*2/*c*	10.063	14.450	14.524	11.8	45	1.846
CAP-AEI2	$(R3)Co_2Al_4P_6O_{24}$	*C*2/*c*	13.735	12.874	18.767	10.8	45	1.792

ticularly advantageous in that they are also highly soluble, even for large molecular weights.

Overview of the large-pore structures. We have synthesized more than a dozen new large-pore materials in seven different ternary systems, all of which have large cages interconnected by multidimensional 12-ring channels. Together with the zeolite rho analogs (Table 1), these large-pore phases raise the concentration limits for Mn and Mg in zeolite type structures. To our knowledge, the replacement of as many as 50% of the Al^{3+} atom sites in aluminophosphate zeolite type structures with Mg^{2+} or Mn^{2+} cations is unprecedented (*13*), and there have been no single-crystal structural studies of any Mn^{2+}-containing zeolite type structures that unambiguously demonstrate the incorporation of Mn^{2+} into the framework T-atom sites (*14*).

Compared to aluminophosphates, it is relatively difficult to make gallophosphate zeolite type structures. Some success in this area has been through the use of the fluoride media (F^-) (*15*). The difference between gallophosphates and aluminophosphates in their ability to form zeolite type structures can be reduced through the incorporation of other elements. A few cobalt gallophosphates are already known (*16*). Recently, we synthesized over a dozen metal (Zn^{2+}, Co^{2+}, and Mg^{2+}) gallophosphates (or arsenates) (*7*, *17*), all of which have metal aluminophosphate analogs. Four large-pore metal gallophosphates are reported here. Among these, the creation of ternary systems with large-pore structures, for example, magnesium gallophosphates, is particularly encouraging. These gallophosphates have extended zeolite type structures into previously unknown compositional domains.

In all of the large-pore structures reported here, M^{3+} (M = Al or Ga) and M^{2+} (M = Co, Mn, Mg, or Zn) cations are far from being evenly distributed among crystallographically unique metal atom sites according to the average M-O distance for each T-atom site: Some metal sites are rich in M^{2+}, whereas others are rich in M^{3+}. Metal sites rich in Ga^{3+}, Mg^{2+}, and Mn^{2+} are sometimes five-coordinate; the fifth ligand, which is 2.2 to 2.6 Å from the corresponding metal atom site, is probably a water molecule.

In the following discussion, the structures are grouped according to framework topology rather than chemical composition. The crystallographic data are listed in Table 1. These materials were made hydrothermally at 180°C with reaction times between 3 and 5 days. Starting materials included $[(CH_3)_2CHO]_3Al$, $Ga(NO_3)_3{\cdot}xH_2O$ or $Ga_2(SO_4)_3{\cdot}xH_2O$, $CoCO_3{\cdot}xH_2O$, $MnCO_3$, $Zn(NO_3)_2{\cdot}6H_2O$, $MgHPO_4{\cdot}3H_2O$, and 85% H_3PO_4. The product chemical compositions derived from the elemental analysis are closely correlated with the average M-O distances in these structures. As expected, M-O distances for the mixed M^{2+} and M^{3+} sites are intermediate between those of M^{2+}-O and M^{3+}-O bonds (*7*, *18*).

UCSB-6. The UCSB-6 family comprises metal (Co, Mn, Mg, or Zn) alumino- (or gallo-) phosphates with a framework topology possessing a 3D 12-ring channel system. The family also includes various forms of crystal structures with different guest species. Crystals are typically hexagonal plates (or prisms) with the largest dimension around 150 μm. However, for some analogs, such as UCSB-6Co and UCSB-6GaCo, much larger crystals (≈600 μm) have been grown. UCSB-6 can be made with several different amines, including 1,7-diaminoheptane, 1,8-diaminooctane, and 1,9-diaminononane. Dipropylamine and diisopropylamine are used as co-solvents in the synthesis with 1,8-diaminooctane and 1,9-diaminononane, respectively, to enhance the solubility of the latter two amines and to provide additional control of the pH. UCSB-6Mg can also be synthesized using 1,10-diaminodecane and dipropylamine. The sample of UCSB-6Co prepared from 1,7-diaminoheptane was pure according to optical microscopy, x-ray powder diffraction, and elemental analysis. Depending on the nature of the metal atoms, UCSB-6 can occur as either a major or a minor phase when amines longer than 1,7-diaminoheptane are used.

With about 45% of the Al^{3+} sites replaced by Co^{2+}, UCSB-6Co has the highest framework transition-metal concentration of any large-pore zeolite type structure. Such a high substitution level is evident from the average M-O bond distance and is supported by a full elemental analysis. The molar ratio of 1 for (Al + Co)/P indicates that there are no extra-framework T-atoms. Such a high transition-metal concentration could lead to novel catalytic and magnetic properties, but it also contributes to the lower thermal stability of UCSB-6 as compared to Al^{3+}-rich molecular sieves. Further studies are needed to examine the stability of this family of compounds and to determine if amines can be removed without loss of the framework structure.

A basic structural unit is the cancrinite cage [the *can* cage (Fig. 1A)], which exists in several zeolite structures, including cancrinite, erionite, and offretite. There are two ways of joining two cancrinite cages with double 6-ring units (D6R): In the so-called symmetrical configuration (Fig. 1C), the two cages are related by a mirror plane, whereas in the "nonsymmetrical" configuration (Fig. 1D), they are related by an inversion center. We use (m)-*can*-D6R-*can* to represent the symmetrical configuration and (i)-*can*-D6R-*can* for the nonsymmetrical one.

The members of the UCSB-6 family consist of (m)-*can*-D6R-*can* units identical to that found in the medium-pore wenkite structure and the large-pore LTL type structure. The cross-linking of (m)-*can*-D6R-*can* units generates the LTL type structure with a 1D 12-ring channel. In UCSB-6, the (m)-*can*-D6R-*can* unit is symmetrically capped with six additional T-atoms at each end to form what we call the capped (m)-*can*-D6R-*can* unit (Fig. 1C). The structure of UCSB-6 consists of columns of capped (m)-*can*-D6R-*can* units cross-linked to others by oxygen bridges. The framework can also be considered as the hexagonal packing of capped (m)-*can*-D6R-*can* units (ABAB sequence) with their long axes aligned along the hexagonal *c* axis.

As a result of these capping T-atoms, the 12-ring window facing the crystallographic *c* direction is less planar than that in zeolite L (Fig. 2, A and C). However, these capping T-atoms are responsible for the formation of three other planar and circular 12-ring windows (free diameter of 8.0 Å, based

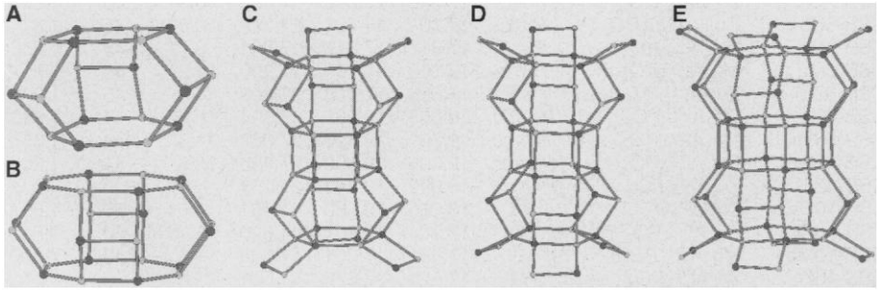

Fig. 1. (**A**) The *can* cage in UCSB-6 and UCSB-10, (**B**) the *ocn* cage in UCSB-8, (**C**) the capped (m)-*can*-D6R-*can* unit in UCSB-6, (**D**) the capped (i)-*can*-D6R-*can* unit in UCSB-10, and (**E**) the capped (m)-*ocn*-D8R-*ocn* unit in UCSB-8. The larger and darker circles represent cobalt (or aluminum) sites; the smaller circles represent phosphorus sites. As in all of the figures, the bridging oxygen atoms are omitted.

on the structure of UCSB-6Co and an oxygen radius of 1.35 Å) facing the directions that are perpendicular to the *c* axis.

The 3D 12-ring channel system of UCSB-6 is similar to that found in the EMT type structure, even though the basic structural building units are different. The structure of UCSB-6 can be derived from the EMT type structure by simply replacing the sodalite cage with the one-sided capped cancrinite cage. Note that the sodalite cage and the one-sided capped cancrinite cage have the same number of T-atoms (24 T-atoms), and thus, the resulting framework has a low T-atom density (12.8 T-atoms per 1000 $Å^3$ for UCSB-6GaCo). This density is comparable to that of the EMT type structure (12.9) and is significantly lower than that of other large-pore structures containing cancrinite cages (for example, 16.7 for cancrinite and 16.4 for zeolite L). Also like the EMT type structure, UCSB-6 has two different large cages: One is bound with five 12-rings, and the other, with three (Fig. 2, A and B). The relation between UCSB-6 (cancrinite cage) and the EMT type (sodalite cage) is evidenced by the similarity in unit cell parameters and space groups (for EMC-2, an aluminosilicate possessing the EMT type structure, a = 17.3 Å and c = 28.8 Å; for UCSB-6Co, a = 17.7 Å and c = 27.3 Å). The space group of UCSB-6 ($P\bar{3}1c$) is a subgroup of that of EMC-2 ($P6_3/mmc$). This relation can be explained by the lack of Al and Si ordering in EMC-2 and the lower symmetry of the capped cancrinite cage as compared with the sodalite cage.

In UCSB-6 structures, there are two extra-framework atomic sites (N atom sites) that are as ordered as the framework O atoms. Except for one or two C atoms adjacent to the N atoms, all other C atoms are highly disordered. The most appropriate reason for the strong ordering of N atoms is that the terminating NH_2 groups are held to the framework by relatively strong N–H···O hydrogen bonds. The shortest N···O distance, of less than 3 Å, supports the presence of N–H···O hydrogen bonds. The similar N and C atom ordering is also found in the UCSB-8 and UCSB-10 structures. The formation of N–H···O hydrogen bonds is an important aspect in the self-assembly of these materials. Factors that affect the making of N–H···O hydrogen bonds include the number of atoms separating two N atoms and the number of hydrogen atoms on each N atom.

UCSB-8. Crystals of UCSB-8 are typically grown as square plates (sometimes with four truncated corners) with a typical dimension of about 150 μm. Structures with several divalent metals (Co, Mn, or

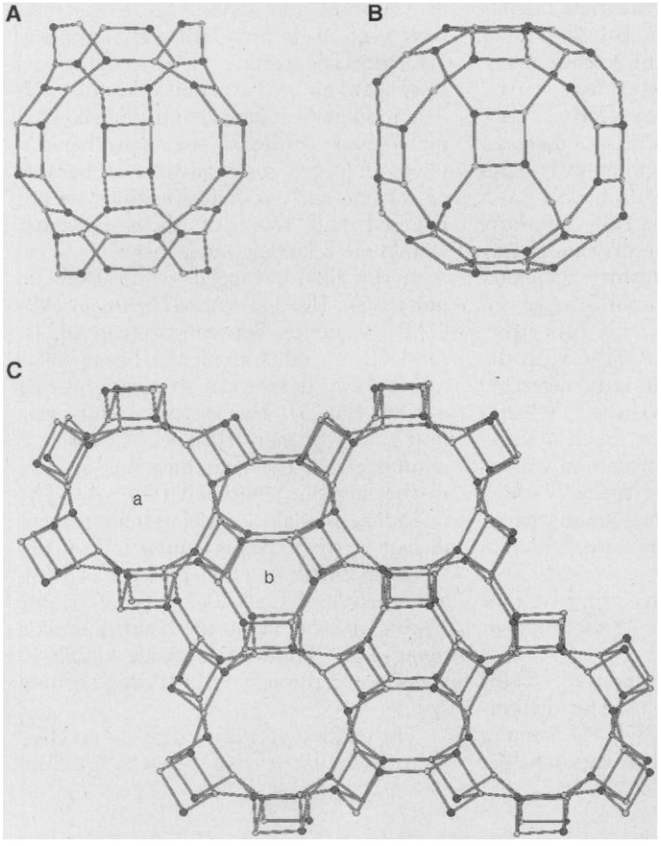

Fig. 2 (left). The large cages in UCSB-6 bound with (**A**) five 12-ring windows or (**B**) three 12-ring windows. (**C**) The 12-ring channels viewed down the *c* axis in UCSB-6. The locations of cages shown in (A) and (B) are marked a and b in (C).

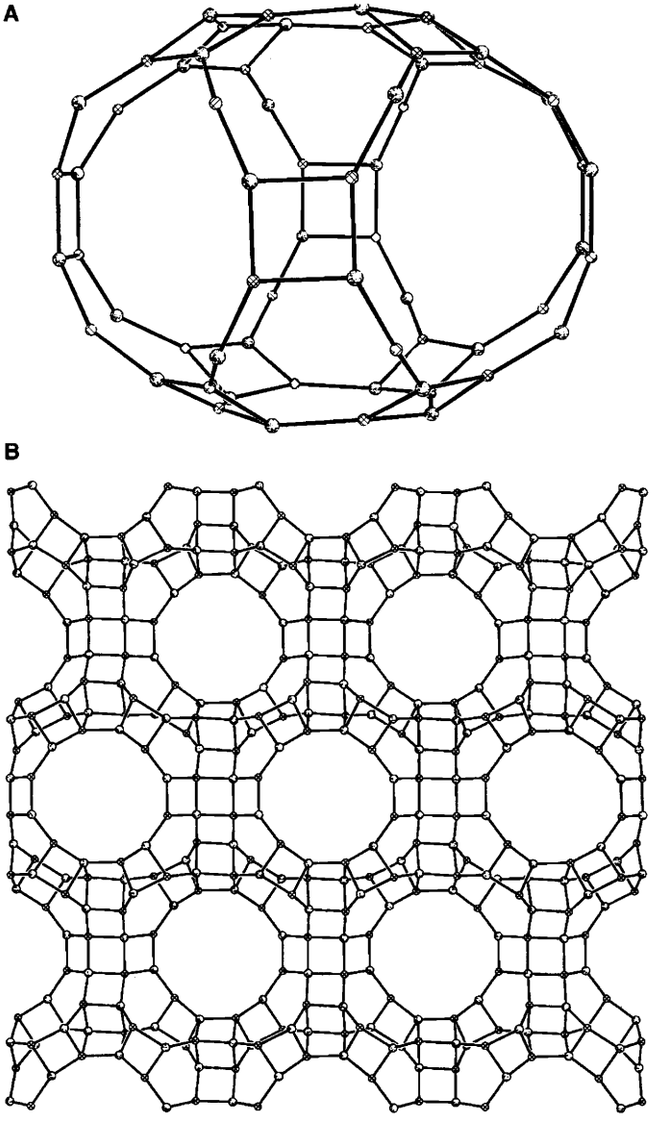

Fig. 3 (right). (**A**) The large cage built from 64 T-atoms and bound with four 12-ring windows in UCSB-8. (**B**) The 12-ring channels viewed down the *a* or *b* axis in UCSB-8.

Mg) have been prepared with 1,9-diaminononane or 1,10-diaminodecane with dipropylamine as co-solvent. Because the use of 1,9-diaminononane and dipropylamine in the zinc aluminophosphate system gives UCSB-6Zn, the polyether diamine route described below has been used to synthesize UCSB-8Zn. The UCSB-8 structures are pseudo–body-centered and could be solved in several body-centered space groups such as *I4/m* with *R* (residual) factors below 10%, but metal atom and P atom sites could not be distinguished. The strict alteration of metal atom and P atom sites is obvious when refinements are performed in space group *P4/nnc*.

The UCSB-8 materials consist of an orthogonal channel system with 12-ring apertures in two dimensions and 8-ring apertures in the third (Fig. 3B). The 12-ring pore size in UCSB-8Co is 7.7 Å by 7.5 Å, slightly smaller than that found in UCSB-6Co. These channels intersect at the center of a large cage (Figs. 3A and 4) consisting of 64 T-atoms (four 12-rings and two 8-rings). The cage measures 20 Å by 20 Å by 15 Å, as measured between oxygen centers using positional coordinates of UCSB-8Co. In comparison, the supercage in faujasite and the α cage in zeolite A have only 48 T-atoms, and two cages in the hexagonal faujasite structure have 60 and 36 T-atoms.

In addition to double 8-rings (D8R), previously known to exist only in merlinoite, paulingite, and zeolite rho, UCSB-8 has a cage consisting of 24 T-atoms. This cage, intermediate between the cancrinite cage (18 T-atoms) and the paulingite cage (32 T-atoms), was first found in the structure of MAPO-39 and has been labeled as an *ocn* cage (Fig. 1B) (*19*). In UCSB-8, two *ocn* cages are symmetrically linked through D8R to give a (m)-*ocn*-D8R-*ocn* unit. Eight additional T-atoms are then symmetrically added to the end 8-rings to give what we call a capped (m)-*ocn*-D8R-*ocn* unit (Fig. 1E). The framework structure consists of columns of capped (m)-*ocn*-D8R-*ocn* units cross-linked to others by oxygen bridges. Alternatively, the framework can be considered as the body-centered packing of capped (m)-*ocn*-D8R-*ocn* units with their long axes aligned along the *c* axis. Other zeolite structures based on the body-centered packing of polyhedral units include ACP-1, with double 4-ring units, and zeolite rho, with α cages (*7*).

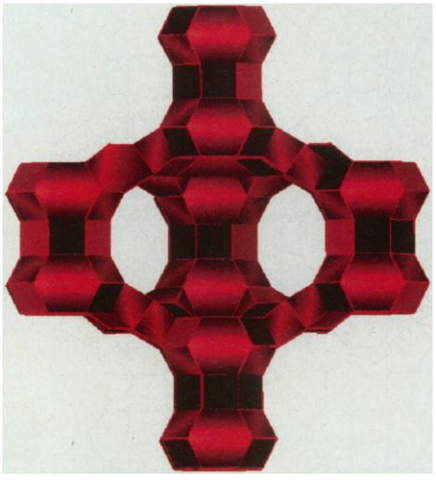

Fig. 4. Cross-sectional view of the 64 T-atom cage surrounded by *ocn* cages and double 8-ring units in UCSB-8.

The size of the large cage in UCSB-8 is related to its structural building units. In UCSB-8, the number of T-atoms of the largest cage is equal to the number of T-atoms in the capped (m)-*ocn*-D8R-*ocn* unit. This observation also applies to UCSB-6 and some other zeolite structural types. For example, the supercage of faujasite and the α cage of zeolite A have the same number of T-atoms as β-D6R-β and β-D4R-β units, respectively (β refers to the sodalite cage). In the two structures reported here, expansion of the capped (m)-*can*-D6R-*can* unit into the capped (m)-*ocn*-D8R-*ocn* increases the size of the largest cage from 48 T-atoms in UCSB-6 to 64 T-atoms in UCSB-8.

UCSB-10. In nature, two cancrinite cages across the D6R unit can be related by either a mirror symmetry (perlialite with LTL structure) or an inversion center (erionite with ERI structure). The synthesis of UCSB-6 with the capped (m)-*can*-D6R-*can* unit suggested that a structure with the capped (i)-*can*-D6R-*can* unit should exist. Such a structure has been made and structurally characterized. Its crystals are typically thick hexagonal plates with a maximum dimension of 1 mm. The structures are refined in space group $R\bar{3}$, but some crystals with different compositions have primitive unit cells, possibly as a result of twinning or pseudosymmetry.

The strategy for the synthesis of UCSB-10 is an extension of that used for the synthesis of UCSB-6 and UCSB-8. As diamines with the hydrophobic carbon backbone get longer, they become less soluble under our synthesis conditions. Ordered rhombohedral lamella phases with interlayer distances ranging from 17 Å (one third of the *c* axis) for the 1,9-diaminononane phase (a = 16.60 Å, c = 51.56 Å) to 20.7 Å for the 1,12-diaminododecane phase (a = 16.50 Å, c = 62.09 Å) become competing products. To enhance the solubility, we used polyether-based diamines with a more hydrophilic backbone. For the synthesis of UCSB-10, different polyether amines with a molecular weight (or average molecular weight) between 170 and 240 are effective.

Single-crystal structure studies showed that UCSB-6 and UCSB-8 type structures can also be formed when only polyether diamines are used. For example, whereas 4,7,10-trioxa-1,13-tridecanediamine or 4,9-dioxa-1,12-dodecanediamine results in the formation of UCSB-10GaZn, either ethylene glycol bis(3-aminopropyl) ether or 1,7-diaminoheptane leads to the crystallization of UCSB-6GaZn; UCSB-8Mn structures have been made from either 4,7,10-trioxa-1,13-tridecanediamine or ethylene glycol bis(3-aminopropyl) ether in addition to 1,9-diaminononane. Compared to the alkyldiamine-based synthesis, the polyether-diamine route has some advantages because co-solvents such as dipropylamines are not required and some of these polyether amines are relatively inexpensive.

In UCSB-10, capped (i)-*can*-D6R-*can* units (Fig. 1D) are stacked with an AB-CABC sequence. Between two capped (i)-*can*-D6R-*can* units along the hexagonal *c* axis are two large cages sharing a 12-ring window (Fig. 5). This structure results in a long *c* axis of more than 41 Å, which is reminiscent of the body diagonal distance in the faujasite cubic cell (≈43 Å). The multidimensional channel system perpendicular to the *c* axis is similar to that observed in UCSB-6, with a pore size of 7.6 Å by 7.4 Å in UCSB-10Co. However, the 12-ring channel along the *c* axis follows a zigzag path. Thus, cages inside UCSB-10 are accessed through a 3D 12-ring channel system.

The relation between UCSB-10 and faujasite is similar to that between UCSB-6

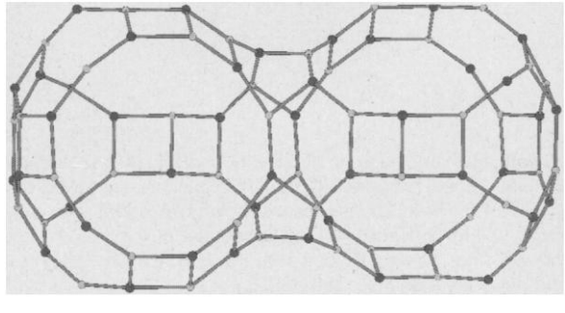

Fig. 5. Two large cages sharing a common 12-ring window in UCSB-10. Each cage is bound with four 12-rings.

and the EMT type structure. Like the supercage in faujasite, the large cage in UCSB-10 is bound with four 12-rings tetrahedrally distributed. The structure of UCSB-10 can be obtained from the faujasite type by replacing the sodalite cage with the one-sided capped cancrinite cage. Such a relation becomes obvious if a rhombohedral unit cell is used to describe the cubic faujasite structure. For example, the cubic cell of a faujasite analog, CAP-FAU1, can be transformed into a rhombohedral cell with a = 17.54 Å and c = 42.95 Å, which becomes very similar to the unit cell of UCSB-10Co (a = 17.70 Å, c = 41.69 Å). A noticeable difference is that faujasite and EMT structures have c axes that are more than 1 Å longer than those of the corresponding UCSB-6 and UCSB-10 structures. This difference has allowed the screening of a large number of crystals grown under various synthesis conditions by determination of unit cell parameters only.

Future directions. The compositional domains achieved in this study imply that there might exist a large family of zeolite type structures not yet synthesized. Some of these unknown phases should be accessible with use of the approach developed here. Such work could open up new areas of research in the synthesis of zeolite type materials. The availability of large single crystals for many related large-pore structures containing different metal cations and protonated amines provides an opportunity to study in detail the coordination chemistry of metal atoms in the zeolite type framework and the structure-directing effects of amines, which should provide guidance for the future design of molecular sieves. The observed correlation between pore geometry and framework charge density is supported by the successful synthesis of UCSB-6, UCSB-8, and UCSB-10 structures with a variety of chemical compositions. It is suggested that a design strategy that allows the expansion of the cagelike structural subunits can lead to even larger cages and a lower framework T-atom density.

REFERENCES AND NOTES

1. W. M. Meier, D. H. Olson, Ch. Baerlocher, *Atlas of Zeolite Structure Types* (Elsevier, Boston, MA, 1996); H. van Bekkum, E. M. Flanigen, J. C. Jansen, Eds., *Introduction to Zeolite Science and Practice* (Elsevier, Amsterdam, 1991); D. W. Breck, *Zeolite Molecular Sieves* (Wiley, New York, 1974).
2. M. E. Davis, C. Saldarriaga, C. Montes, J. Garces, C. Crowder, *Nature* **331**, 698 (1988); R. M. Dessan, J. L. Schlenker, J. B. Higgins, *Zeolites* **10**, 552 (1990); C. C. Freyhardt, M. Tsapatsis, R. F. Lobo, K. J. Balkus Jr., M. E. Davis, *Nature* **381**, 295 (1996).
3. R. H. Richard *et al.*, *J. Solid State Chem.* **102**, 204 (1993); M. Estermann, L. B. McCuster, C. Baerlocher, A. Merrouche, H. Kessler, *Nature* **352**, 320 (1991).
4. M. I. Khan *et al.*, *Chem. Mater.* **8**, 43 (1996).
5. T. R. Gaffney, *Curr. Opin. Solid State Mater. Sci.* **1**, 69 (1996).
6. L. B. McCuster, in *Comprehensive Supramolecular Chemistry*, G. Alberti and T. Bein, Eds. (Elsevier, New York, 1996), vol. 7, pp. 393–423.
7. P. Feng, X. Bu, G. D. Stucky, *Nature* **388**, 735 (1997).
8. M. E. Davis and S. I. Zones, in *Synthesis of Porous Materials, Zeolites, Clays, and Nanostructures*, M. L. Occelli and H. Kessler, Eds. (Dekker, New York, 1996), pp. 1–34.
9. J. M. Bennett and B. K. Marcus, in *Innovation in Zeolite Materials Science*, P. J. Grober, W. J. Mortier, E. F. Vansant, G. Schulz-Ekloff, Eds. (Elsevier, New York, 1980), pp. 269–279; P. A. Wright *et al.*, *J. Chem. Soc. Chem. Commun.* **1993**, 633 (1993).
10. P. Feng, X. Bu, G. D. Stucky, *Angew. Chem. Int. Ed. Engl.* **34**, 1745 (1995).
11. Q. Huo *et al.* *Science* **268**, 1324 (1995).
12. Diamines, $NH_2(CH_2)_nNH_2$ ($7 \leq n \leq 12$), have been used for some time in the synthesis of microporous materials and are known to be the structure-directing agents in the crystallization of multidimensional high-silica zeolites ZSM-5 and ZSM-11 [E. W. Valyocsik and L. D. Rollmann, *Zeolites* **5**, 123 (1985)].
13. S. T. Wilson and E. M. Flanigen, in *Zeolite Synthesis*, M. L. Occelli and H. E. Robson, Eds. (ACS Symposium Series 398, American Chemical Society, Washington, DC, 1989), pp. 329–345.
14. The crystal structure of $MnPO_4$-11 was reported; however, the concentration of Mn is too low to have an effect on the structural refinement [J. J. Pluth *et al.*, *J. Phys. Chem.* **92**, 2734 (1988)].
15. H. Kessler, J. Patarin, C. Schott-Darie, in *Studies in Surface Science and Catalysis*, J. C. Jansen, M. Stocker, H. G. Karge, J. Weitkamp, Eds. (Elsevier, New York, 1994), vol. 85, pp. 75–113.
16. A. M. Chippindale and A. R. Cowley, *Zeolites* **18**, 176 (1997).
17. X. Bu, T. E. Gier, P. Feng, G. D. Stucky, *Microporous Mater.*, in press.
18. R. D. Shannon, *Acta Crystallogr. A* **32**, 751 (1976).
19. L. B. McCuster, G. O. Brunner, A. F. Oju, *ibid.* **46**, C55 (1990); K. J. Andries and J. V. Smith, in preparation.
20. Synthesis procedures and analytical data are available at http://www.sciencemag.org/feature/data/974117.shl. We thank Q. Huo for helpful discussions and D. Pierce from the Department of Geological Sciences for help with the electron probe microanalysis. This work was supported in part by the National Science Foundation under grant DMR 95-20971 and the U.S. Army Research Office under grant DAAH04-96-1-0443. A Materials Research Laboratory Corning Foundation Fellowship for P.F. is gratefully acknowledged.

14 August 1997; accepted 7 November 1997

Immune Versus Natural Selection: Antibody Aldolases with Enzymic Rates But Broader Scope

Carlos F. Barbas III,* Andreas Heine, Guofu Zhong, Torsten Hoffmann, Svetlana Gramatikova, Robert Björnestedt, Benjamin List, James Anderson, Enrico A. Stura, Ian A. Wilson,* Richard A. Lerner*

Structural and mechanistic studies show that when the selection criteria of the immune system are changed, catalytic antibodies that have the efficiency of natural enzymes evolve, but the catalytic antibodies are much more accepting of a wide range of substrates. The catalytic antibodies were prepared by reactive immunization, a process whereby the selection criteria of the immune system are changed from simple binding to chemical reactivity. This process yielded aldolase catalytic antibodies that approximated the rate acceleration of the natural enzyme used in glycolysis. Unlike the natural enzyme, however, the antibody aldolases catalyzed a variety of aldol reactions and decarboxylations. The crystal structure of one of these antibodies identified the reactive lysine residue that was selected in the immunization process. This lysine is deeply buried in a hydrophobic pocket at the base of the binding site, thereby accounting for its perturbed pK_a.

The central dilemma in the development of alternative protein catalysts concerns duplicating the rate accelerations of natural enzymes while increasing their versatility. For new enzymes to be optimally useful in chemistry, they must be both efficient and capable of accepting various substrates. Whereas the need for efficiency is obvious, the scope problem arises because enzymes would be more useful if they could catalyze a class of reactions with diverse substrates. To solve this problem, we have used antibody catalysis.

The approach is best highlighted by comparing the processes by which evolution and the immune system develop new protein functions. During evolution natural selection occurs as a consequence of improved function or fitness. In the case of

The authors are at The Skaggs Institute for Chemical Biology and the Department of Molecular Biology, The Scripps Research Institute, 10550 North Torrey Pines Road, La Jolla, CA 92037, USA.

*To whom correspondence should be addressed.